Spectroscopy of molecular states in a few–electron double quantum dot

A.K. Hüttel [a,1], S. Ludwig [a], K. Eberl [b,2], J.P. Kotthaus [a]

[a] Center for NanoScience and Department Physik, Ludwig–Maximilians–Universität, Geschwister–Scholl–Platz 1, 80539 München, Germany

[b] Max-Planck-Institut für Festkörperforschung, Heisenbergstraße 1, 70569 Stuttgart, Germany

Abstract

Semiconductor quantum dots, so-called artificial atoms, have attracted considerable interest as mesoscopic model systems and prospective building blocks of the "quantum computer". Electrons are trapped locally in quantum dots, forming controllable and coherent mesoscopic atom- and moleculelike systems. Electrostatic definition of quantum dots by use of top gates on a GaAs/AlGaAs heterostructure allows wide variation of the potential in the underlying two-dimensional electron gas. By distorting the trapping potential of a single quantum dot, a strongly tunnel-coupled double quantum dot can be defined. Transport spectroscopy measurements on such a system charged with N=0,1,2,... electrons are presented. In particular, the tunnel splitting of the double well potential for up to one trapped electron is unambiguously identified. It becomes visible as a pronounced level anticrossing at finite source drain voltage. A magnetic field perpendicular to the two-dimensional electron gas also modulates the orbital excitation energies in each individual dot. By tuning the asymmetry of the double well potential at finite magnetic field the chemical potentials of an excited state of one of the quantum dots and the ground state of the other quantum dot can be aligned, resulting in a second level anticrossing with a larger tunnel splitting. In addition, data on the two-electron transport spectrum are presented.

Introduction

Electrostatically defined semiconductor double quantum dots [1] have over the recent years attracted a large amount of interest originating from different motivations. On one hand, quantum dots and cou- pled quantum dots provide a fully tunable mesoscopic model system as "artificial atoms" [1] and "artificial molecules" [2,3], respectively. Electrons are trapped locally in externally controllable potential wells. In addition, transport spectroscopy allows direct observation of many fundamental quantum-mechanical phenomena, ranging e.g. from shell filling [4] and molecular hybridization [5–7] to interaction with the crystal lattice [8,9] and coherent motion of electrons [10,11]. On the other hand several proposals for using the charge or spin states of electrons trapped in quantum dots as qubits, the elementary registers of the proposed quantum computer, have emerged. Foremost,

the use of a single electron spin provides a well-defined two-level system [12]. In addition, several other differing schemes for using quantum dots in quantum information processing have been proposed [11,13–15].

The material system in use is a AlGaAs/GaAs heterostructure, forming a two-dimensional electron gas (2DEG) 120 nm below the crystal surface. The electron sheet density of the 2DEG at $T \simeq 4.2\,\mathrm{K}$ is $n_s \simeq 1.8 \times 10^{15}\,\mathrm{m}^{-2}$, the electron mobility $\mu \simeq 75\,\mathrm{m}^2/\mathrm{Vs}$. Using optical and e-beam lithography, gate electrodes are deposited on the chip surface. When a negative voltage is applied to these electrodes with respect to the 2DEG, the Schottky barrier between metal and semiconductor prevents current. For a sufficiently negative gate voltage, the electrical field however raises the conduction band edge in the 2DEG locally near the electrode above the Fermi energy, leading to a depletion of the 2DEG. Using several gate electrodes ("split gates") and adapting the electrode geometry, conducting islands within an otherwise non-conducting crystal are formed – the electrostatically defined quantum dots.

1. Distortion of a quantum dot into a double quantum dot

Figure 1(a) displays a SEM micrograph of the gate geometry that has been used in the measurements. The 2DEG itself is contacted outside the depicted region, where Ohmic contacts have been formed via germanium n^+ doping [16]. The confinement potential within the plane of the 2DEG is generated by four gate electrodes, marked with g_L, g_R, g_C, and g_X. Two tunnel barriers, between gates g_L and g_X, or g_R and g_X, respectively, connect the quantum dot to the 2DEG forming the source (S) and drain (D) leads. The shape of the gate electrodes, adapted from a geometry first published in Ref. [17], is optimized such that the size of the quantum dot and thereby the number of trapped electrons can be decreased strongly while still maintaining a measurable tunnel rate to the leads. It has been shown that this and similar gate geometries allow to measure a single electron tunneling (SET) current even in the limit of only one trapped electron in the quantum dot [17,18].

In addition, gates g_R and g_{QPC} as marked in Fig. 1(a) can be used to define a quantum point contact (QPC),
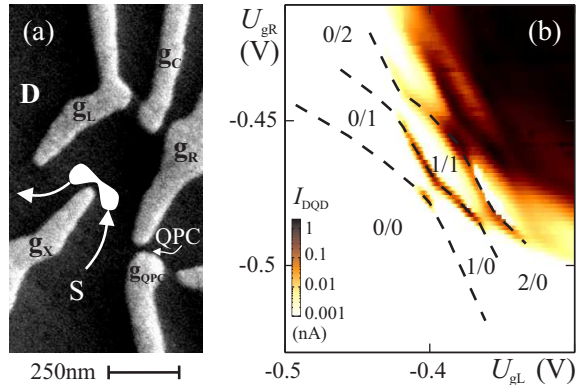

Fig. 1. (a) SEM micrograph of the gate electrode geometry used to define a double quantum dot (DQD) and a quantum point contact (QPC). The approximate positions of DQD and QPC and the current paths are indicated in white. (b) Current through the DQD as function of the side gate voltages U_{gL} and U_{gR} ($U_{SD,dc} = 50\,\mu\mathrm{V}$, logarithmic color scale). The black dashed lines trace the gate voltages where the total charge in the DQD changes by $1e$, as detected by the quantum point contact [7].

i.e. a one-dimensional constriction of the 2DEG. Conductance quantization leads here for specific gate voltage ranges to a strong dependence of the tunnel current through the QPC on the local electrostatic potential [19,20]. The QPC can thus be used as a charge sensor, detecting a change of the number of electrons in the nearby quantum dot [18,21,22].

Measurements of the transport spectrum of the quantum dot as well as the QPC charge detection prove that the charge of the observed quantum dot can be controlled all the way down to a total electron number $N = 1$. In the few electron limit the electronic shell structure within the confinement potential becomes clearly visible [4,23]. In addition, the confinement potential can be shaped via adjustments of the top gate voltages. Thus, by application of increasingly negative gate voltages on the center gates U_{gC} and U_{gX}, accompanied by appropriate balancing of the voltages on the side gates U_{gL} and U_{gR}, the electronic trapping potential can be distorted into a double well potential [7,23,24]. This way, a double quantum dot is shaped. During the deformation process, the Coulomb blockade oscillations can be traced. Between the gate voltages marking SET current the number of trapped electrons remains constant, thereby disclosing the charge of the resulting double quantum dot.

A charge stability diagram of the strongly coupled

double quantum dot is displayed in Fig. 1(b). Here, the linear response dc current ($U_{SD} = 50\,\mu V$) is plotted as a function of the side gate voltages U_{gL} and U_{gR}. Dashed lines mark gate voltages where the QPC detects a change of the total charge in the double quantum dot. In the lower left region of the plot no further changes in charge occupation are observed, confirming that here the double quantum dot is completely emptied of conduction band electrons [7].

The regular pattern of the stability diagram shows areas of stable charge configurations caused by Coulomb blockade, where the electron numbers in both quantum dots are fixed. In a double quantum dot having weak interdot coupling these areas correspond to pronounced hexagons [25,26]. The strong tunnel coupling within the double quantum dot present in this particular measurement, however, causes a rounding of the hexagon edges by means of the sizable hybridization energy [2]. Such an "artificial molecule" forms delocalized symmetric (bonding) and antisymmetric (antibonding) states.

In a weakly tunnel-coupled double quantum dot, the electron number in Coulomb blockade is a fixed integer in each dot. Then, SET current through a serial double quantum dot is only possible when the electron number can fluctuate in both quantum dots, as at the triple points of the stability diagram [26]. Here, three charge configurations are energetically degenerate. In the case of strong tunnel coupling between the two dots, however, the delocalized molecular states carry SET current. Hence, current is detected along the hexagon edges of the stability diagram, along which two charge configurations are degenerate, as can be observed in Fig. 1(b).

2. One-electron transport spectrum

The transport spectrum in linear response, measured with a very small source drain voltage, provides access only to the quantum mechanical ground state of each charge configuration. For obtaining information on excited states, the source-drain voltage U_{SD} has to be sufficient to provide electrons with an excess kinetic energy larger then the excitation energy. At finite U_{SD} each triple point of the charge stability diagram expands in a characteristic way into a larger region
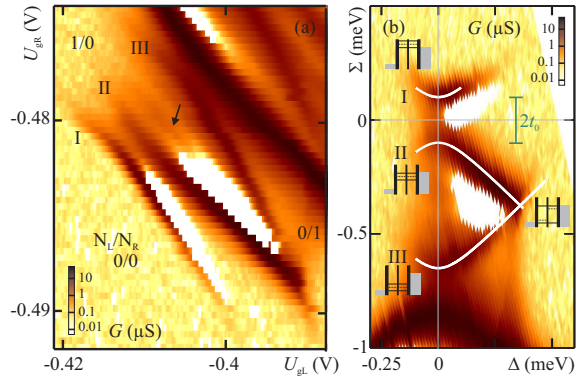

Fig. 2. (a) Differential conductance of the double quantum dot, as function of the side gate voltages U_{gL} and U_{gR}, around the first triple point of the stability diagram near charge configurations $N_L/N_R = 0/0$, $1/0$, $0/1$. A large source-drain voltage $U_{SD} = -0.75\,mV$ is applied. (b) The same data, plotted in the intrinsic coordinate system of the double quantum dot (average energy Σ of the double well potential and potential asymmetry Δ, see text). The model expectations for a two-state system are overlayed.

where SET current can be observed. For weak tunnel coupling, these regions form a triangular shape in the stability diagram [26–28]. A differential conductance measurement observes the edges of the triangles.

Fig. 2(a) displays the differential conductance of our double quantum dot at strong tunnel coupling, for an applied source-drain voltage $U_{SD} = -0.75\,mV$. In contrast to the expectation for weak interdot tunnel coupling the lines of finite differential conductance observed here do not trace a single triangle. Instead, the first triple point of the stability diagram, where the charge configurations with electron numbers in the left and right quantum dot $N_L/N_R = 0/0$, $0/1$, and $1/0$ contribute to transport, expands into three lines marked I, II, and III. The distance between lines I and III is increasing with source-drain voltage. As is also confirmed by dc current measurements (data not shown), along line I the transport window of finite SET current opens. Thus, here the chemical potential corresponding to the molecular ground state is aligned with the Fermi edge of the 2DEG in the source contact. Along line III, the transport windows closes again, as the ground state chemical potential is aligned with the drain chemical potential. Note that by chosing the energy zero, we can assume this chemical potential

$$\mu_+(1) \equiv E_+(1) - E(0) = E_+(1) + \text{const.} \quad (1)$$

3

to be equal the molecular ground state energy $E_+(1)$, since the energy of the empty quantum dot $E(0)$ can be assumed constant.

Line II of enhanced differential conductance in between lines I and III has to correspond to the opening of an additional transport channel via an excited state. Its meaning becomes immediately clear when plotting the measured data in an intrinsic coordinate system of the double quantum dot. This has been done in Fig. 2(b), where the same measurement data as in Fig. 2(a) is plotted after applying a linear coordinate transformation. Using additional calibration measurements as well as the data presented here, the influence of each gate voltage U_{gL} and U_{gR} on the chemical potentials for adding an electron in the left quantum dot μ_L and for adding an electron in the right quantum dot μ_R has been calculated. The two axes now designate the average potential in the two dots $\Sigma = (\mu_L + \mu_R)/2$ and the potential asymmetry $\Delta = (\mu_R - \mu_L)/2$.

As can be seen in Fig. 2(b), lines I and II form a level anticrossing as function of the potential asymmetry Δ. They obviously correspond to the symmetric ground state and the antisymmetric excited state of the single electron double quantum dot. The anticrossing is well described as a function of the potential asymmetry Δ by

$$E_\pm(1) = \mp\sqrt{\Delta^2 + t_0^2} \qquad (2)$$

defining the white model lines in Fig. 2(b), where $2t_0 = 0.2\,\text{meV}$ is the tunnel splitting.

The identification of these lines of enhanced differential conductance enables us to obtain the dependence of the tunnel splitting on external parameters in a straightforward way. Since the distance between lines I and III of enhanced conductance corresponds to the energy scale of the externally supplied and controlled source-drain voltage, it provides a means of energy calibration. By comparing it to the minimum distance between lines I and II in the same direction in one of the plots of Fig. 2 and linearly scaling the energy, the tunnel splitting is obtained. This can be done for both the raw data (Fig. 2(a)) and the data after coordinate transformation (Fig. 2(b)), since the linear transformation preserves the length ratio. Other characteristic energy values, as e.g. the charging energy for the second electron E_2, can be measured in a similar way.

In addition, information on the time-averaged electron number within the SET region can be extracted
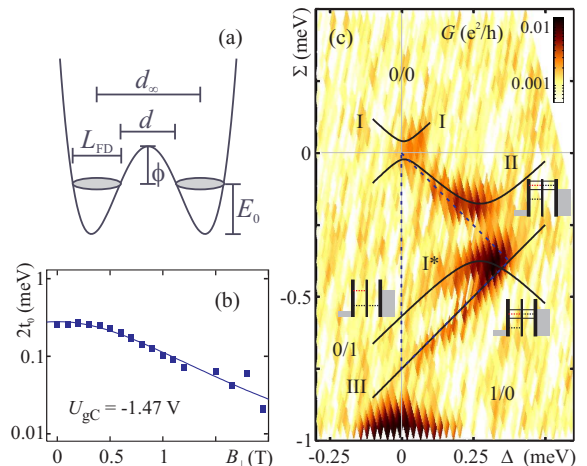

Fig. 3. (a) Scheme of the WKB model for the dependence of the tunnel splitting on an increasing magnetic field perpendicular to the 2DEG $B_\perp$, detailing the symbols used in the text. (b) Measured dependence of $2t_0$ on $B_\perp$. The solid line corresponds to a model curve (see text). (c) Tunnel spectrum of the double quantum dot at $B_\perp = 1.4\,\text{T}$. Differential conductance G as function of the intrinsic energies Σ and Δ, displaying a second level anticrossing at high potential asymmetry.

by observing the quantum point contact charge detection. Since the effective tunnel rates into and out of the double quantum dot depend on both the tunnel barrier properties and the probability density of the electronic wavefunction, by varying Δ and thereby shifting the wavefunction information on the transmittance of the tunnel barriers coupling the double quantum dot to the leads is obtained [7].

3. One-electron transport spectrum at high magnetic field

Applying a magnetic field $B_\perp$ perpendicular to the 2DEG modifies the transport spectrum. The decreasing magnetic length $L_B = \sqrt{\hbar/|e|\,B_\perp}$ causes a compression of the electronic wave functions. Thus, the effective tunnel rate through all tunnel barriers in the nanoscale structure decreases. This leads to a uniform decrease of SET current, which is partly due to the shrinking of the molecular tunnel splitting. Fig.3(a) displays a double well potential, where the center barrier of effective amplitude ϕ defines the interdot tunnel splitting. We now introduce a simple model to describe

4

the effect of a perpendicular magnetic field $B_\perp$ on the interdot tunnel splitting. The center of charge distance d_∞ of the two quantum dots is assumed to be independent of $B_\perp$. The size of the quantum dots shrinks in a perpendicular magnetic field, and approaches L_B when the magnetic length becomes smaller than the geometrical confinement of the quantum dots. Thus, the diameter of both quantum dots is assumed to scale with the Fock-Darwin length [29]

$$L_{\mathrm{FD}} = \frac{L_{\mathrm{B}}}{\sqrt[4]{1 + 4\omega_0^2/\omega_c^2}}, \qquad (3)$$

where ω_0 describes the harmonic oscillator potential and $\omega_c = |e| B_\perp/m^*$ is the cyclotron frequency. This defines a magnetic field dependent "effective tunnel barrier width"

$$d(B_\perp) = d_\infty - L_{\mathrm{FD}}(B_\perp). \qquad (4)$$

Inserting this expression into the WKB approximation yields a functional dependence for the tunnel splitting $2t_0(B_\perp)$. Fig. 3(b) displays the measured tunnel splitting as well as a model curve (solid line) with ω_0, d_∞, and ϕ as fit parameters [7]. The agreement with our data is satisfactory.

A magnetic field perpendicular to the 2DES not only leads to magnetic compression of the quantum states, but also modifies the orbital level spectrum. In our case for $B_\perp \gtrsim 1\,\mathrm{T}$, an additional excited state enters the transport window defined by the source-drain voltage [30], as shown in Fig. 3(c) for $B_\perp = 1.4\,\mathrm{T}$. Here, the excited state becomes visble as new line of enhanced conductance marked with I*. Remarkably, for a large potential asymmetry $\Delta \simeq 0.275\,\mathrm{meV}$, a second level anticrossing involving lines I* and II becomes visible. Whereas the tunnel splitting $2t_0 = 0.064\,\mathrm{meV}$, as obtained in Ref. [7] for the ground state – ground state hybridization, is already strongly decreased at $B_\perp = 1.4\,\mathrm{T}$, for this second level anticrossing the splitting remains $2t_0^* \simeq 0.2\,\mathrm{meV}$. The energy level diagrams that are shown as insets in Fig. 3(c) illustrate the origin of the observed second anticrossing. In this case, the ground state of one of the quantum dots and an excited state of the other dot are energetically aligned, leading to hybridized molecular states. Consistently, this is also observed when measuring dc current, where delocalization causes a significant increase in SET tunneling, and in the QPC signal (data not shown).

The situation involving both single dot ground states and one additional excited state can be modeled by the Hamiltonian

$$\mathcal{H} \doteq \begin{pmatrix} \Delta & -t_0 & -t_0^* \\ -t_0 & -\Delta & 0 \\ -t_0^* & 0 & -\Delta + \epsilon^* \end{pmatrix}, \qquad (5)$$

where Δ and $2t_0$ again describe the ground state two-level system. The excitation energy in one of the two quantum dots is given by ϵ^* and the tunnel splitting caused by hybridization between this excited state and the ground state of the other dot is $2t_0^*$. The model curves in Fig. 3(c) (solid lines) corespond to this Hamiltonian for $2t_0 = 0.064\,\mathrm{meV}$, $2t_0^* = 0.2\,\mathrm{meV}$, and $\epsilon^* = 0.55\,\mathrm{meV}$. They show good agreement with the measured data. [3]

4. Two-electron transport spectrum

A large body of theoretical literature has been dedicated to the level spectrum of a double quantum dot occupied with two electrons, the "quantum dot hydrogen molecule" [12,31–34]. This is to a considerable extent due to the proposed use of the spin exchange coupling for realizing controlled two-spin interaction, or "two-qubit gates". The ground state for $N = 2$ is at zero magnetic field expected to be a singlet, the first excited states are given by three spin-degenerate triplet states. In both cases the two electrons are predominantly distributed over the double quantum dot. The energy difference between singlet and triplet is the effective Heisenberg exchange coupling J. Time-resolved experiments have recently been successfully used for quantifying J in the weak coupling limit [11]. However, few data on direct dc observation of the two electron levels in GaAs in the strong coupling case is published.

Figure 4(a) displays a measurement of the transport spectrum near the triple point for degenerate charge configurations $N_L/N_R = 1/0 \leftrightarrow 0/1 \leftrightarrow 1/1$. Here, the charge of the symmetric double quantum dot varies between one and two electrons. By means of the voltage on gate g_C, which couples nearly equally to both

---

[3] The actual value of the parameter $2t_0 = 0.064\,\mathrm{meV}$ is taken from magnetic field dependent measurements shown in Ref. [7] that also take into account the data of Fig. 3(c).
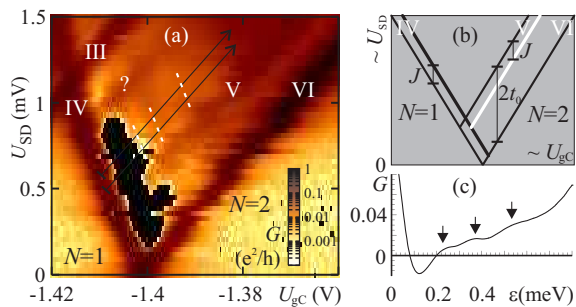
Fig. 4. (a) Differential conductance G of the strongly coupled double quantum dot, as function of U_{gC} and U_{SD}, for $1 \leq N \leq 2$ electrons. Constant values for U_{gL} and U_{gR} are chosen such that the double well potential is approximately symmetric. Isolated black regions mark negative differential conductance. (b) From Ref. [32]: Theoretical expectations for this parameter region. (c) Averaged trace through the measurement of (a), showing regular lines of enhanced conductance (see text).

quantum dots, the electrostatic potential in both dots is varied simultaneously keeping the double quantum dot approximately symmetric. A gradual modification of $2t_0$ is naturally expected in this case and has been observed. In addition, U_{SD} can influence the potential asymmetry Δ. A detailed treatment of these effects is however outside the scope of this article. In Fig. 4(a) the conductance is plotted as function of U_{SD} and U_{gC}, displaying diamond-shaped regions of Coulomb blockade similar as in the case of a single quantum dot.

From comparisons with measurements as shown in Fig. 2, the three dominant lines of enhanced differential conductance can be unambiguously identified. At line IV, the two-electron ground state enters the transport window. The source-drain voltage provides sufficient energy that even an energetically lower-lying electron can leave the quantum dot, such that the dot remains in the excited antisymmetric one-electron state. Along line V, this second transport channel is "switched off", meaning that only the molecular ground states for $N = 1$ and $N = 2$ electrons contribute to transport. Line VI then again corresponds to the transition into Coulomb blockade with $N = 2$. Thus, these main features directly mirror the data of the first triple point. At the left edge of the plot, at high source-drain voltage line III of the first triple point becomes visible, bordering the two electron tunneling region.

Figure 4(b) displays the theoretical expectations for the transport spectrum in this parameter region un-

der the condition $2t_0 \ll \hbar\omega_0$, as presented in Ref. [32]. As stated previously, for the first triple point the energy of the one-electron molecular states can be treated synonymously with the associated chemical potential $\mu(1) = E(1) - E(0) = E(1) + \text{const}$. Here, the chemical potential that has to be aligned with the source or drain Fermi edge is given by the relation

$$\mu(2) = E(2) - E(1), \qquad (6)$$

with $E(2)$ as a two-electron eigenenergy and $E(1)$ as a one-electron eigenenergy. Thus, both the one and two electron level spectra are expected to be visible in transport. The triplet states separated by the exchange energy J from the singlet state result for certain conditions in a second line of finite differential conductance parallel to both line IV and V [32].

A comparison of experiment (Fig. 4(a)) and theory (Fig. 4(b)) displays significant differences. In the measurement data of Fig. 4(a), the additional line marked "?" with an excitation engergy $\Delta\epsilon > 2 \times 2t_0$ probably corresponds to a higher orbital one-electron excitation. In the lower-energy range, a pronounced region of negative differential conductance becomes visible. Although excited states are observed, a unique identification has not been possible for most of the lines that involve two electron states. Clearly our data do not allow the identification of the exchange coupling J. A possible reason for this is that the confinement potential is already quite shallow for the more positive gate voltages U_{gC} required to reach $1 \leq N \leq 2$. For $0 \leq N \leq 1$ a higher excited orbital state can e.g. be observed at an excitation energy $\Delta\epsilon \sim 0.4\,\text{meV}$, as indicated in Fig. 2(a) with a black arrow. At the gate voltages present in the $1 \leq N \leq 2$ region, however, a nearly regular pattern of two-electron excited states with excitation energies $\Delta\epsilon \sim 0.2\,\text{meV}, \ 0.4\,\text{meV}, \ 0.55\,\text{meV}$ is found. While difficult to recognize in the raw data of Fig. 4(a), where the corresponding resonances are indicated with white dashed lines, they can be easily seen in the line plot of Fig. 4(c). Here, the differential conductance along multiple traces through Fig. 4(a) starting from line IV and parallel to line VI (as indicated by the black arrows) is averaged. One-electron resonances run parallel to line VI and are therefore not visible in the line plot, whereas two-electron resonances occur at fixed distances to line IV and are emphasized by this averaging. Assuming that these regularly spaced resonances correspond to orbital excitations within the single quantum dot po-

tential wells and thereby $\hbar\omega_0 \sim 0.2\,\mathrm{meV} \lesssim 2t_0$, further level hybridizations can take place, and a complex level spectrum is expected.

Because of the strong tunnel coupling between the double quantum dot and its leads, it has been possible to observe Kondo-enhanced differential conductance for the one, two, and three electron case in the presented double quantum dot. More details will be published in the near future [35].

Summary and acknowledgements

Measurements on a strongly coupled double quantum dot are presented. It is defined by deforming the confinement potential of a single quantum dot in the two-dimensional electron gas of a GaAs/AlGaAs heterostructure. For $N = 1$ trapped electron, the excitation energy of the first molecular orbital excited state displays a distinct level anticrossing with the ground state. This enables the direct identification of the symmetric molecular ground state and the antisymmetric molecular excited state of the double well potential in transport spectroscopy.

The effect of a magnetic field $B_\perp$ perpendicular to the 2DEG is discussed. Magnetic compression of the wavefunction leads to a decrease in tunnel splitting, which can be modeled using the WKB approximation. At high field $B_\perp = 1.4\,\mathrm{T}$ and high potential asymmetry, a second level anticrossing becomes visible when an excited state of one quantum dot hybridizes with the ground state of the other dot. Further, data on the two-electron transport spectrum of the double quantum dot are presented, where the strong coupling and level broadening prevents a non-ambiguous identification of the quantum states.

References

[1] R. C. Ashoori, Nature 379 (1996) 413.

[2] R. H. Blick, D. Pfannkuche, R. J. Haug, K. von Klitzing, K. Eberl, Phys. Rev. Lett. 80 (18) (1998) 4032.

[3] T. H. Oosterkamp, T. Fujisawa, W. G. van der Wiel, K. Ishibashi, R. V. Hijman, S. Tarucha, L. P. Kouwenhoven, Nature 395 (1998) 873.

[4] S. Tarucha, D. G. Austing, T. Honda, R. J. van der Hage, L. P. Kouwenhoven, Phys. Rev. Lett. 77 (17) (1996) 3613.

[5] R. H. Blick, R. J. Haug, J. Weis, D. Pfannkuche, K. von Klitzing, K. Eberl, Phys. Rev. B 53 (12) (1996) 7899.

[6] A. W. Holleitner, R. H. Blick, A. K. Hüttel, K. Eberl, J. P. Kotthaus, Science 297 (5578) (2002) 70.

[7] A. K. Hüttel, S. Ludwig, H. Lorenz, K. Eberl, J. P. Kotthaus, Phys. Rev. B 72 (2005) 081310(R).

[8] T. Fujisawa, T. H. Oosterkamp, W. G. van der Wiel, B. W. Broer, R. Aguado, S. Tarucha, L. P. Kouwenhoven, Science 282 (5390) (1998) 932.

[9] K. Ono, S. Tarucha, Phys. Rev. Lett. 92 (25) (2004) 256803.

[10] T. Hayashi, T. Fujisawa, H. D. Cheong, Y. H. Jeong, Y. Hirayama, Phys. Rev. Lett. 91 (22) (2003) 226804.

[11] J. R. Petta, A. C. Johnson, J. M. Taylor, E. A. Laird, A. Yacoby, M. D. Lukin, C. M. Marcus, M. P. Hanson, A. C. Gossard, Science 309 (5744) (2005) 2180.

[12] D. Loss, D. P. DiVincenzo, Phys. Rev. A 57 (1) (1998) 120.

[13] A. Barenco, D. Deutsch, A. Ekert, R. Jozsa, Phys. Rev. Lett. 74 (20) (1995) 4083.

[14] T. Tanamoto, Phys. Rev. A 61 (2000) 022305.

[15] W. G. van der Wiel, T. Fujisawa, S. Tarucha, L. P. Kouwenhoven, Jap. J. Appl. Phys. 40 (2001) 2100.

[16] N. Braslau, J. Vac. Sci. Techn. 19 (3) (1981) 803.

[17] M. Ciorga, A. S. Sachrajda, P. Hawrylak, C. Gould, P. Zawadzki, S. Jullian, Y. Feng, Z. Wasilewski, Phys. Rev. B 61 (24) (2000) 16315.

[18] J. M. Elzerman, R. Hanson, J. S. Greidanus, L. H. Willems van Beveren, S. D. Franceschi, L. M. K. Vandersypen, S. Tarucha, L. P. Kouwenhoven, Phys. Rev. B 67 (16) (2003) 161308.

[19] D. A. Wharam, T. J. Thornton, R. Newbury, M. Pepper, H. Ahmed, J. E. F. Frost, D. G. Hasko, D. C. Peacock, D. A. Ritchie, G. A. C. Jones, J. Phys. C 21 (8) (1988) L209.

[20] B. J. van Wees, H. van Houten, C. W. J. Beenakker, J. G. Williamson, L. P. Kouwenhoven, D. van der Marel, C. T. Foxon, Phys. Rev. Lett. 60 (9) (1988) 848.

[21] M. Field, C. G. Smith, M. Pepper, D. A. Ritchie, J. E. F. Frost, G. A. C. Jones, D. G. Hasko, Phys. Rev. Lett. 70 (9) (1993) 1311.

[22] D. Sprinzak, Y. Ji, M. Heiblum, D. Mahalu, H. Shtrikman, Phys. Rev. Lett. 88 (17) (2002) 176805.

[23] A. K. Hüttel, K. Eberl, S. Ludwig, submitted for publication, cond-mat/0607248 (2006).

[24] L. Gaudreau, S. A. Studenikin, A. S. Sachrajda, P. Zawadzki, A. Kam, J. Lapointe, M. Korkusinski, P. Hawrylak, Phys. Rev. Lett. 97 (3) (2006) 036807.

[25] F. Hofmann, T. Heinzel, D. A. Wharam, J. P. Kotthaus, G. Böhm, W. Klein, G. Tränkle, G. Weimann, Phys. Rev. B 51 (19) (1995) 13872.

[26] W. G. van der Wiel, S. D. Franceschi, J. M. Elzerman, T. Fujisawa, S. Tarucha, L. P. Kouwenhoven, Rev. Mod. Phys. 75 (1) (2003) 1.

[27] D. Dixon, L. P. Kouwenhoven, P. L. McEuen, Y. Nagamune, J. Motohisa, H. Sakaki, Phys. Rev. B 53 (19) (1996) 12625.

[28] A. C. Johnson, J. R. Petta, C. M. Marcus, M. P. Hanson, A. C. Gossard, Phys. Rev. B 72 (16) (2005) 165308.

[29] L. Jacak, P. Hawrylak, A. Wójs, Quantum Dots, Springer–Verlag, 1998.

[30] A. K. Hüttel, S. Ludwig, H. Lorenz, K. Eberl, J. P. Kotthaus, Physica E 34 (2006) 488.

[31] G. Burkard, D. Loss, D. P. DiVincenzo, Phys. Rev. B 59 (3) (1999) 2070.

[32] V. N. Golovach, D. Loss, Phys. Rev. B 69 (24) (2004) 245327.

[33] X. Hu, S. Das Sarma, Phys. Rev. A 61 (2000) 062301.

[34] W. Dybalski, P. Hawrylak, Phys. Rev. B 72 (20) (2005) 205432.

[35] D. M. Schröer, A. K. Hüttel, K. Eberl, S. Ludwig, M. N. Kiselev, B. L. Altshuler, submitted for publication, cond-mat/0607044 (2006).